Surface energy and spatial dispersion in ferroelectrics: the influence on the optical transmission and reflection spectra in the paraelectric state

2004 J. Phys.: Condens. Matter 16 1849

(http://iopscience.iop.org/0953-8984/16/10/016)

INSTITUTE OF PHYSICS PUBLISHING JOURNAL OF PHYSICS: CONDENSED MATTER

J. Phys.: Condens. Matter **16** (2004) 1849–1870 PII: S0953-8984(04)72284-5

Surface energy and spatial dispersion in ferroelectrics: the influence on the optical transmission and reflection spectra in the paraelectric state

Jean-Pierre Jardin and Philippe Moch

Laboratoire des Propriétés Mécaniques et Thermodynamiques des Matériaux, CNRS, Institut Galilée, Université Paris-Nord, Avenue J-B Clément, 93430 Villetaneuse, France

Received 19 November 2003
Published 27 February 2004
Online at stacks.iop.org/JPhysCM/16/1849 (DOI: 10.1088/0953-8984/16/10/016)

Abstract

The description of surface and size effects in ferroelectrics is based on the combined contribution of surface free energy density and gradient dependent terms occurring in the volume free energy density. The dynamics of the polarization waves and, consequently, the optical properties in the infrared range, can be significantly affected in the case of small enough soft mode damping, even in the paraelectric phase at temperatures above those of the ordered ferroelectric state. Reflection and transmission spectra for semi-infinite media and thin films are calculated within this model, using the orders of magnitude generally published in the literature for ferroelectric oxides as regards the values of the physical parameters. It is shown that the tangential and the normal interface extrapolation lengths, as well as the bulk gradient coefficient related to the model studied, could be subjected to a spectroscopical evaluation. The frequencies of the sharp singularities appearing in the transmission and reflection spectra are given with an excellent precision by the frequencies of the surface and of the guided modes calculated in the electrostatic approximation for wavevector equal to zero, thus providing a rather simple way of determining the pertinent physical quantities.

1. Introduction

Size effects in ferroelectrics materials have been, since the 1970s, a subject of theoretical and experimental interest and are still, for the time being, of importance due to the integration of nanosized ferroelectric oxides into microelectronic devices. In particular it is generally expected that surfaces, in small particles or in thin films, will induce a variation of the polarization field in their neighbourhood with consequences for the critical temperature for ferroelectric transition [1–10] and the question of a critical thickness in thin films for the existence of ferroelectricity remains a subject of current interest [11].

A microscopic effective Hamiltonian, based on first-principles calculations, was recently used to give some insight into this last question [12, 13], but until now most of the theoretical studies on low size ferroelectrics were made in the framework of the modified phenomenological Landau–Devonshire theory. This is performed by the addition of:

(i) a gradient term $(S/2)|\nabla P|^2$ in the free energy density to take into account the non-homogeneity of the polarization,
(ii) a surface energy term, generally described by introduction of an 'extrapolation length' Δ which can be positive or negative (Δ positive (negative) involves a decrease (increase) of the polarization at the surface).

To our knowledge there has been no direct experimental evaluation of the value of Δ; the only available values are the ones given by Wang *et al* chosen to fit the Curie temperatures of small particles and used after them by other authors [7–10]. Recently Chew *et al* proposed far infrared reflection (FIR) measurements to determine surface and size effects in ferroelectric thin films [14, 15] arguing that, in their calculations, the effects of Δ on the reflection curves are qualitatively different, and can be distinguished from those induced by the coefficient S of the gradient term. Indeed a physical consequence of the introduction of a gradient term in the free energy density is to make the ferroelectric a spatially dispersive medium (the dielectric constant depends on the wavevector). So, as discussed in detail by Maradudin and Mills [16] in a calculation of the reflectivity of the surface of a semi-infinite dielectric medium with spatial dispersion, there are, in the case of a TE incident plane wave, two polariton modes (or three in the case of TM incident light) which propagate or not in the medium, depending on the incident wave frequency. In particular, at normal incidence, a wave with a large wavevector can propagate in the usual stop band between the transverse optical frequency and the longitudinal one, and can, on one hand, reduce the reflectivity in the low frequency side of the stop band and, on the other hand, give rise to interference fringes in the film which works like a Fabry–Perot interferometer [14]. In their study, Chew *et al* emphasize the distinctly different effects of the parameters S and Δ on the position and on the intensity of the fringes appearing in the restrahlung band of the ferroelectric. However, they do not consider the effect of Δ on the reflection curves in the paraelectric phase and they admit that the results obtained in the case $\Delta^{-1} = 0$ could be extended to any value of Δ. This appears to be in contradiction with the results that we have presented in previous papers [17, 18], in which we have shown that, in a dielectric with spatial dispersion and surface energy terms, polarization waves propagating along the surface of a semi-infinite medium or in the plane of a slab have dispersion relations which depend on the value and on the sign of the parameter Δ.

So the purpose of the present paper is to explore in detail the effect of Δ on the optical reflectivity and transmissivity of ferroelectric materials, in the paraelectric phase, within the scope of the Landau–Ginzburg theory discussed in [17], using parameters roughly related to ferroelectric oxides [11]. In the case of TM incident waves we need two distinct extrapolation lengths Δ_X and Δ_Z, and we obtain closed expressions for the reflectivity in a semi-infinite medium and in thin films. In a semi-infinite medium the reflection curves exhibit sharp singularities at frequencies which are very close to those of surface modes calculated in the electrostatic approximation of [17], but which exist only in the case of negative values of Δ_X or Δ_Z. In the case of thin films, with the parameters used we do not observe the fringes exhibited by Chew *et al* because of the very large values of the wavevector of the wave which propagates in the restrahlung region, but for small enough film thickness the reflection and transmission curves present singularities at frequencies close to those of the guided modes obtained in the electrostatic approximation. And again, in the case where Δ_X and Δ_Z are negative, singularities at frequencies close to those of surface waves can be observed.

In section 2 we begin with a review of the main features of our calculation. In section 3, results are presented and discussed for reflectivity in a semi-infinite system in the TE and TM geometries (section 3.1), and for reflectivity and transmission for free thin films or films on a dielectric substrate in the same geometries (section 3.2). In each case we show that the frequencies of the singularities which appear in the reflection curves can be approximated with great accuracy by surface or guided mode frequencies.

2. Theoretical approach

2.1. Description of the system studied

In the following we use a model deriving from a previously discussed one [17] describing surface effects in a spatially dispersive dielectric medium. It is based on the coupling of the Maxwell equations with the Landau–Ginzburg equation of motion of the ionic polarization $\boldsymbol{P}$. The harmonic part of the volume free energy density is written as

$$F_{\mathrm{v}} = \tfrac{1}{2}\sum_i \{\alpha(T - T_{\mathrm{c}})P_i^2 + S(\nabla P_i)^2\} - \mathbf{E}\cdot\boldsymbol{P}. \tag{1}$$

The index i refers to the Cartesian components (X, Y, Z: see figure 1). $\mathbf{E}$ is the macroscopic electric field. The positive constant S provides spatial dispersion. As usual, the first term (in which $\alpha > 0$) induces the conventional ferroelectric phase transition, occurring at T_{c} in the simplified Landau approach. In the following we maintain the temperature T significantly above T_{c}, thus restricting our study to the paraelectric phase and avoiding the complications related to the inhomogeneity of the ferroelectric state. In the medium, the equation of motion for $\boldsymbol{P}$ is then written as

$$m\frac{\partial^2 \boldsymbol{P}}{\partial t^2} + \alpha(T - T_{\mathrm{c}})\boldsymbol{P} + m\Gamma\frac{\partial \boldsymbol{P}}{\partial t} - S\nabla^2\boldsymbol{P} = \mathbf{E}. \tag{2}$$

The positive coefficients m and Γ refer to an inertial and to a damping constant, respectively. We impose a permittivity ε_∞ at very high frequency, related to the electronic polarization, such that the total polarization $\mathbf{P}$ is

$$\mathbf{P} = \boldsymbol{P} + \frac{\varepsilon_\infty - 1}{4\pi}\mathbf{E}. \tag{3}$$

The system studied, presented in figure 1, refers to a semi-infinite spatially dispersive dielectric medium ($Z > 0$) or to a slab of thickness D ($-D/2 < Z < D/2$). In the semi-infinite case, we assume the presence of a conventional homogeneous dielectric medium of permittivity ε_1 for $Z < 0$. The slab is supposed to be surrounded by two generally distinct conventional homogeneous dielectric media of permittivity ε_1 ($Z < -D/2$) and ε_2 ($Z > D/2$), respectively: $\varepsilon_1 = \varepsilon_2 = 1$ corresponds to a film surrounded by vacuum; $\varepsilon_1 = 1$, $\varepsilon_2 \neq 1$ corresponds to a film lying on a substrate. Each interface induces a surface free energy density which allows one to define a tangential ($\Delta_{X,(1,2)} = \Delta_{Y,(1,2)}$) and a normal ($\Delta_{Z,(1,2)}$) extrapolation length, as pointed out in a previous paper [17]. For instance, in the case of a slab, the values of these interface free energy densities $F_{\mathrm{s}1}$ and $F_{\mathrm{s}2}$ are written as

$$F_{\mathrm{s}1} = \sum_i \frac{S}{\Delta_{i,1}}(P_i^2)_{Z=-D/2}; \qquad F_{\mathrm{s}2} = \sum_i \frac{S}{\Delta_{i,2}}(P_i^2)_{Z=+D/2}. \tag{4}$$

There result boundary conditions related to these surface terms; namely, for a slab,

$$\left[\frac{\partial P_i}{\partial Z} - \frac{P_i}{\Delta_{i,1}}\right]_{Z=-D/2} = 0; \qquad \left[\frac{\partial P_i}{\partial Z} + \frac{P_i}{\Delta_{i,2}}\right]_{Z=+D/2} = 0. \tag{5}$$

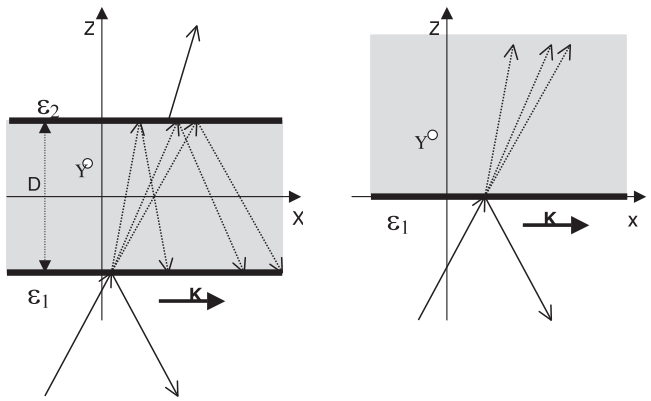

Figure 1. Schematic diagrams of the systems studied.

2.2. Derivation of the optical properties

These are calculated with the help of the equation of motion, of Maxwell equations and of boundary conditions derived from expressions (5) and from electromagnetic general considerations. At any point in the space the electromagnetic fields consist of linear combinations of (generalized) plane waves of common frequency Ω and of wavevector showing a common in-plane real component K: Ω and K are fixed by an imposed incident wave of wavevector $\mathbf{K_i}\{K, 0, Q_i\}$ with $Q_i = (\varepsilon_1\Omega^2/c^2 - K^2)^{1/2}$, where c is the velocity of light in vacuum. We characterize the optical properties by the ratio r of the amplitudes of the reflected wave (of wavevector $\mathbf{K_r}\{K, 0, -Q_i\}$) and of the incident one.

In the medium, it is convenient to define the permittivity $\varepsilon(\Omega, \mathbf{K})$ as a function of Ω and of the wavevector $\mathbf{K}\{K, 0, Q\}$:

$$\varepsilon(\Omega, \mathbf{K}) = \varepsilon(\Omega, K, Q) = \varepsilon_\infty \frac{\Omega_l^2 - \Omega^2 - i\Gamma\Omega + (S/m)(K^2 + Q^2)}{\Omega_t^2 - \Omega^2 - i\Gamma\Omega + (S/m)(K^2 + Q^2)} \tag{6}$$

with

$$\Omega_t^2 = \frac{\alpha(T - T_c)}{m}; \qquad \Omega_l^2 = \Omega_t^2 + \frac{4\pi}{m\varepsilon_\infty}. \tag{7}$$

For further comparison, we also define the reference permittivity ε_b which accounts for the optical properties in the absence of spatial dispersion and of surface effects:

$$\varepsilon_b = \varepsilon_\infty \frac{\Omega_l^2 - \Omega^2 - i\Gamma\Omega}{\Omega_t^2 - \Omega^2 - i\Gamma\Omega}. \tag{8}$$

It results from Maxwell equations that one is faced with two independent kinds of solutions related to TE (or s) and TM (or p) radiation, respectively. The TE solutions refer to electric and polarization fields normal to the plane of incidence, i.e. lying along the Y-axis. The TM solutions refer to electric and polarization fields in the plane of incidence.

It follows from

$$\varepsilon(\Omega, \mathbf{K})\nabla \cdot \mathbf{E} = 0 \tag{9}$$

that the dispersion relations split into two sets:

$$\varepsilon(\Omega, \mathbf{K}) = 0 \qquad \text{or} \qquad \nabla \cdot \mathbf{E} = 0. \tag{10}$$

The cancelling of ε and the Maxwell equations imply that

$$\mathbf{E} = \frac{\mathbf{K}\cdot\mathbf{E}}{\mathbf{K}^2}\mathbf{K} \tag{11}$$

and, consequently, that there is no component of $\mathbf{E}$ along the Y-axis for such a (generalized) longitudinal wave: then, it is not of TE kind. The second set provides the usual dispersion relation for any (generalized) transverse wave:

$$\varepsilon(\Omega, \mathbf{K}) = \frac{c^2\mathbf{K}^2}{\Omega^2} \tag{12}$$

and is found both in TE and TM wave types.

To summarize:

(i) In the TE case, Q^2 can only take two values, Q_1^2 and Q_2^2, in the medium [18]. They are solutions of

$$\varepsilon(\Omega, K, Q) = \frac{c^2(K^2+Q^2)}{\Omega^2}. \tag{13}$$

Expression (13) defines a quadratic equation in Q^2.

(ii) In the TM case, Q^2 can take three values in the medium [18]: Q_1^2, Q_2^2 and, in addition, Q_3^2 with

$$\Omega_1^2 - \Omega^2 - \mathrm{i}\Gamma\Omega + (S/m)(K^2+Q_3^2) = 0. \tag{14}$$

This last equation provides the value Q_3^2 of Q^2 which cancels the permittivity $\varepsilon(\Omega, K, Q)$.

The result is that in a slab, the electromagnetic field is a linear combination of four generalized plane waves for the TE solution and of six generalized plane waves for the TM one. In the case of a semi-infinite medium, Q is subject to the additional condition $\mathrm{Im}(Q) > 0$ and, consequently, the number of waves occurring is reduced to two and three for the TE and for the TM solution, respectively. In every case the explicit value of r can be expressed by solving a set of linear equations, as is detailed further in the appendix. Indeed, the transmission coefficient t can also be easily evaluated. In the absence of damping, Q_1^2, Q_2^2 and Q_3^2 are real; depending upon the sign of Q^2, the associated waves are strictly propagative ($Q^2 > 0$) or show an exponential behaviour along Z ($Q^2 < 0$). In order to make precise the nature of the waves in the medium it is helpful to introduce the bulk transverse polariton frequencies $\Omega_{\mathrm{t}-}(K)$ and $\Omega_{\mathrm{t}+}(K)$; $\Omega_{\mathrm{t}-}^2$ and $\Omega_{\mathrm{t}+}^2$ are the two (always positive) solutions of

$$\varepsilon(\Omega_{\mathrm{t}\pm}, K, 0) = \frac{c^2K^2}{\Omega_{\mathrm{t}\pm}^2}. \tag{15}$$

It can be easily shown that, for $\Omega < \Omega_{\mathrm{t}-}$, Q_1^2 and Q_2^2 are both negative, and that they are both positive for $\Omega > \Omega_{\mathrm{t}+}$; between $\Omega_{\mathrm{t}-}$ and $\Omega_{\mathrm{t}+}$, Q_1^2 is negative and Q_2^2 is positive. In addition, it is convenient to define the bulk longitudinal polariton frequency $\Omega_{\mathrm{lp}}(K)$ which lies between $\Omega_{\mathrm{t}-}(K)$ and $\Omega_{\mathrm{t}+}(K)$:

$$\Omega_{\mathrm{lp}}(K) = \left\{\Omega_1^2 + \frac{SK^2}{m}\right\}^{1/2} \tag{16}$$

Q_3^2 is negative for $\Omega < \Omega_{\mathrm{lp}}$ and positive for $\Omega > \Omega_{\mathrm{lp}}$. Finally, note that, in order to ensure the propagation of an incident wave, one has to achieve $K < \sqrt{\varepsilon_1}(\Omega/c)$ (or, equivalently, $\Omega > cK/\sqrt{\varepsilon_1}$). This condition is obtained at any angle of incidence θ: $K = \sqrt{\varepsilon_1}(\Omega/c)\sin[\theta]$ and $Q_{\mathrm{i}} = \sqrt{\varepsilon_1}(\Omega/c)\cos[\theta]$.

2.3. Simple extensions: attenuated reflection and guided modes

The validity of the expressions obtained for r is not restricted to the case of incident radiation consisting on a conventional propagating electromagnetic plane wave: more generally, they provide the ratio of the amplitudes of two generalized plane waves which are supposed to exist in the dielectric of permittivity ε_1 with wavevectors $\mathbf{K_i}(K, Q_i)$ and $\mathbf{K_r}(K, -Q_i)$ satisfying $K^2 + Q_i^2 = \varepsilon_1(\Omega^2/c^2)$. Negative values of Q_i^2 can be studied: they refer to evanescent waves. Experimentally, such waves can be generated through irradiation with a large enough angle of incidence, via a dielectric medium of permittivity exceeding ε_1 lying under the system at a certain distance. For this geometrical arrangement, the so-called attenuated reflectivity can be easily calculated.

Another application concerns the calculation of the dispersion curves of the surface and (in the case of films) of the guided modes. These polarization waves are defined as excitations showing an exponential decrease outside the spatially dispersive medium studied: such behaviour necessitates a negative Q_i^2 value and, since, by definition, $\mathrm{Im}(Q_i) > 0$, the vanishing of the amplitude of the incident wave related to $\mathbf{K_i}$: thus, if r becomes infinite, the amplitude related to $-Q_i$ (the 'reflected' wave) is allowed to differ from 0, in spite of the null amplitude related to Q_i. In other words, this second condition stipulates that the frequencies of the surface guided modes are derived through the search for the vanishing of r^{-1}, i.e. for the poles of r. An alternative method, based on the cancelling of the determinant of an homogeneous set of linear equations, was previously presented [17]: indeed, it provides identical results, but it is less convenient to use. Let us briefly recall the results:

(i) In the slabs the electrostatic approximation provides excellent evaluations of the frequencies, except at very small K values (typically smaller than a few Ω_t/c) [18]; all the modes, except a TE one and a TM one, show a cut-off value of the wavevector below which they disappear; the cut-off wavevector is related to the frequency by $K = \sqrt{\varepsilon_1}(\Omega/c)$; the TE mode which remains allowed at any wavevector shows a frequency which is practically given by $cK/\sqrt{\varepsilon_1}$ at very small K.

(ii) In the case of a semi-infinite medium there are one TE and one TM surface mode only when $\Delta_X < 0$; the electrostatic approximation provides excellent evaluations of their frequencies $\Omega_s(K)$ but they show a cut-off wavevector which, as expected, corresponds to a frequency identical to $\Omega_{t-}(K)$ (i.e. $\Omega_s(K) = \Omega_{t-}(K)$).

Finally, it is interesting to note that poles of r are also related to the so-called 'virtual radiative modes' which provide an alternative tool for the study of the optical properties [19, 20].

2.4. Choice of the parameters and reduced variables

Our calculations were performed using realistic values of the parameters, close to the usually assumed ones for ferroelectric materials, for instance $BaTiO_3$. These parameters are listed in table 1. We took various sets of extrapolation lengths, including negative values. Up to now, the occurrence of negative values suffers from a lack of completely convincing experimental confirmation. As discussed in the next section, negative values lead to qualitative changes in the reflection and transmission spectra: it then seemed to us useful to anticipate the corresponding calculations in order to attempt to probe their existence experimentally. As regards the damping, it was neglected in a first step, thus allowing an easier discussion. On introducing the damping, we find that, as usual, the singularities are softened: values of $\Omega\Gamma$ not exceeding a few tenths still allow one to observe dispersion and surface effects. However, such a significant underdamping does not always occur: in the case of $BaTiO_3$, for instance,

Table 1. Commonly used values of the parameters.

$\alpha = 10^{-4}$ K^{-1}
$T_c = 400$ K
$\Omega_0 = 10^{13}$ s^{-1} ($\Rightarrow$: $K_0 = 3.33 \times 10^{-5}$ nm^{-1}; $D_0 = 3 \times 10^4$ nm)
$\varepsilon_\infty = 5$
$S = 0.1$ nm^2
$\varepsilon_1 = 1$
$\varepsilon_2 = 1$ or 3 or 5
T: from 480 to 800 K
$\Delta_{X,(1,2)}$: from +3 nm to $+\infty$ and from $-\infty$ to -3 nm
$\Delta_{Z,(1,2)}$: from +3 nm to $+\infty$ and from $-\infty$ to -3 nm
γ: from 0 to 1
d: from 10^{-3} to 1 ($\Rightarrow$ D: from 30 to 3×10^4 nm)

$\Omega\Gamma$ remains larger than 1 in the whole paraelectric phase [21]. We shall show that for large $\Omega\Gamma$ values the surface and dispersion terms affect the spectra negligibly.

In order to study the variations of r and of the reflection coefficient $R = rr^*$ of the intensity, it is convenient to use reduced parameters and variables. Defining Ω_0, K_0 and D_0 as follows:

$$\Omega_0 = cK_0 = c/D_0 = \alpha T_c/m, \tag{17}$$

we introduce the reduced quantities

$$\begin{aligned}
&\omega = \Omega/\Omega_0; \qquad \omega_t = \Omega_t/\Omega_0; \qquad \omega_l = \Omega_l/\Omega_0; \qquad \gamma = \Gamma/\Omega_0;\\
&s = S/(mc^2); \qquad \omega_{t\pm} = \Omega_{t\pm}/\Omega_0; \qquad \omega_{lp} = \Omega_{lp}/\Omega_0; \qquad k = K/K_0;\\
&q_i = Q_i/K_0; \qquad q_1 = Q_1/K_0; \qquad q_2 = Q_2/K_0; \qquad q_3 = Q_3/K_0;\\
&x = X/D_0; \qquad y = Y/D_0; \qquad z = Z/D_0; \qquad d = D/D_0;\\
&\delta_{i,(1,2)} = \Delta_{i,(1,2)}/D_0
\end{aligned} \tag{18}$$

where $i = x, y, z$ or X, Y, Z. In view of further comments concerning the influence of damping it is useful to note that the relative damping γ_r is generally defined as $\gamma_r = \Gamma/\Omega_t$. It results that $\gamma_r = \gamma/\omega_t$. With the values listed in table 1, $\gamma_r = 2.24\gamma$.

In figure 2 we have reported the various domains of interest in an (ω, k) diagram. This figure is drawn using deliberately modified values of the parameters in order to provide a qualitative illustration of the various existing cases: the index P labels the allowed areas in the case of an incident illuminating radiation (a, b and c indicate regions such as $\{Q_1^2 < 0,\ Q_2^2 > 0,\ Q_3^2 < 0\}$, $\{Q_1^2 < 0,\ Q_2^2 > 0,\ Q_3^2 > 0\}$ and $\{Q_1^2 > 0,\ Q_2^2 > 0,\ Q_3^2 > 0\}$, respectively); the index S refers to the occurrence of surface modes ($\{Q_1^2 < 0,\ Q_2^2 < 0,\ Q_3^2 < 0\}$) and, finally, G corresponds to the domains of guided modes (a: $\{Q_1^2 < 0,\ Q_2^2 > 0,\ Q_3^2 < 0\}$; b: $\{Q_1^2 < 0,\ Q_2^2 > 0,\ Q_3^2 > 0\}$).

3. Optical reflection and transmission: results and discussion

3.1. Semi-infinite medium

In the following, we present the reflectivity properties of semi-infinite samples for TE and TM polarizations. They give rise to a rather simple analytical interpretation.

3.1.1. TE propagation. The reflection spectrum does not significantly differ from the one obtained in the case of a conventional dielectric medium with permittivity ε_b given by

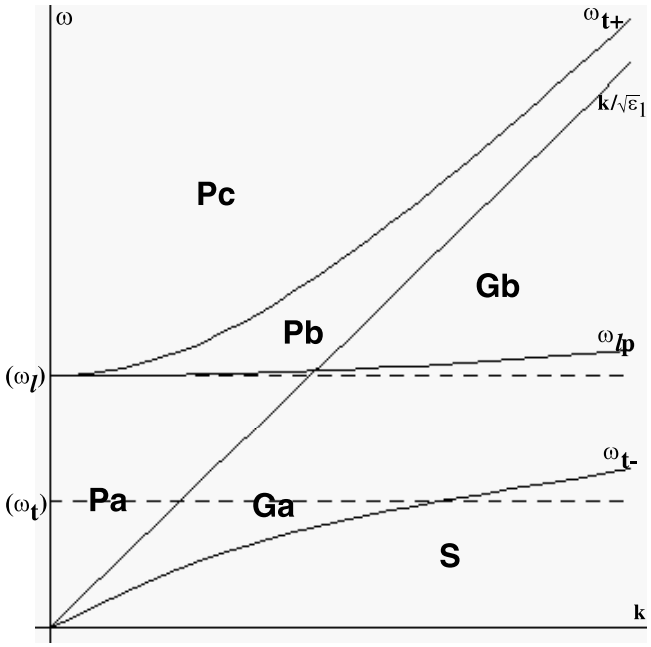

Figure 2. Allowed domains for the different electromagnetic regimes in the k–ω (wavevector–frequency) plane. P: propagation outside the medium studied; S (surface) and G (guided): evanescent behaviour outside the medium studied (for a symmetrically surrounded film). In the S domain: $Q_1^2 < 0$, $Q_2^2 < 0$, $Q_3^2 < 0$. Elsewhere: a $\Leftrightarrow$ $Q_1^2 < 0$, $Q_2^2 > 0$, $Q_3^2 < 0$; b $\Leftrightarrow$ $Q_1^2 < 0$, $Q_2^2 > 0$, $Q_3^2 > 0$; c $\Leftrightarrow$ $Q_1^2 > 0$, $Q_2^2 > 0$, $Q_3^2 > 0$.

equation (8), except, and only when the extrapolation length δ_x is negative, within a small frequency interval, as shown in figures 3 and 4: this change consists in a reflectivity peak which grows up to the value 1 in the absence of damping. Its frequency does not vary with the angle of incidence.

The reflection coefficient for the TE polarization does not depend upon δ_z and is given by

$$r = \frac{(q_\mathrm{i} - q_1)(q_1^2 - g^2)(q_2 + \mathrm{i}/\delta_x) - (q_\mathrm{i} - q_2)(q_2^2 - g^2)(q_1 + \mathrm{i}/\delta_x)}{(q_\mathrm{i} + q_1)(q_1^2 - g^2)(q_2 + \mathrm{i}/\delta_x) - (q_\mathrm{i} + q_2)(q_2^2 - g^2)(q_1 + \mathrm{i}/\delta_x)} \tag{19}$$

where

$$g^2 = \frac{\omega^2 + \mathrm{i}\gamma\omega - \omega_\mathrm{t}^2 - sk^2}{s}. \tag{20}$$

For $\gamma = 0$, q_2 is a real number. It immediately results from (19) that

$$\text{when } q_1 = -\frac{\mathrm{i}}{\delta_x} \qquad r = \frac{q_\mathrm{i} - q_1}{q_\mathrm{i} + q_1} \tag{21}$$

and, therefore, $R = 1$. Note that, due to the condition $\mathrm{Im}(q_1) > 0$, this can be realized only for $\delta_x < 0$. Numerically, the orders of magnitude of the parameters provide a value of the related frequency very close to the frequency ω_{sx} of the TE surface mode at zero wavevector [17], which is written as

$$\omega_{sx} = \left(\omega_\mathrm{t}^2 - \frac{s}{\delta_x^2}\right)^{1/2}. \tag{22}$$

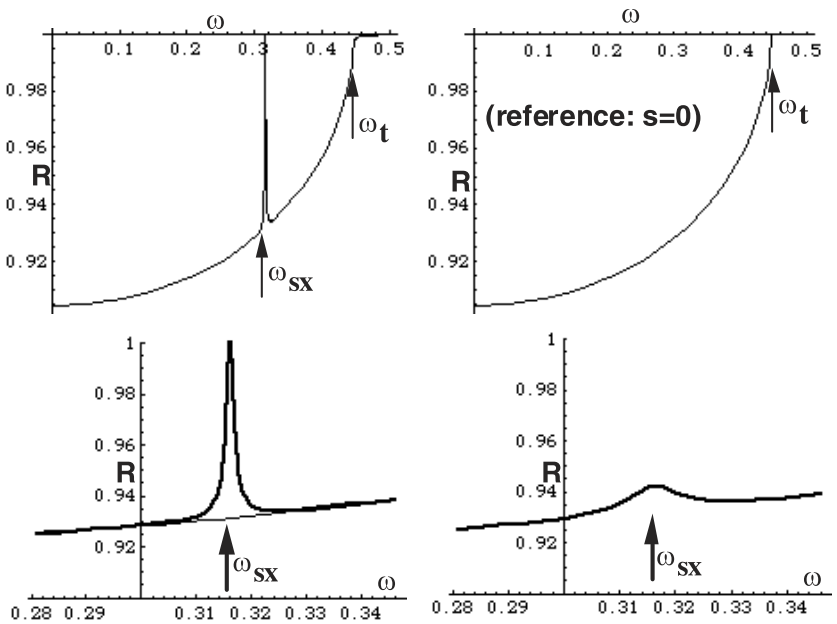

Figure 3. Computed TE reflection spectra for a semi-infinite medium: $\Delta_X = -5$ nm; $\theta = 5°$. Upper row: comparison with the reference spectrum (on the right-hand side: $s = 0 \Leftrightarrow$ permittivity ε_b). Lower row: the detailed effect of damping (left column: $\gamma = 0$; right column: $\gamma = 0.01$).

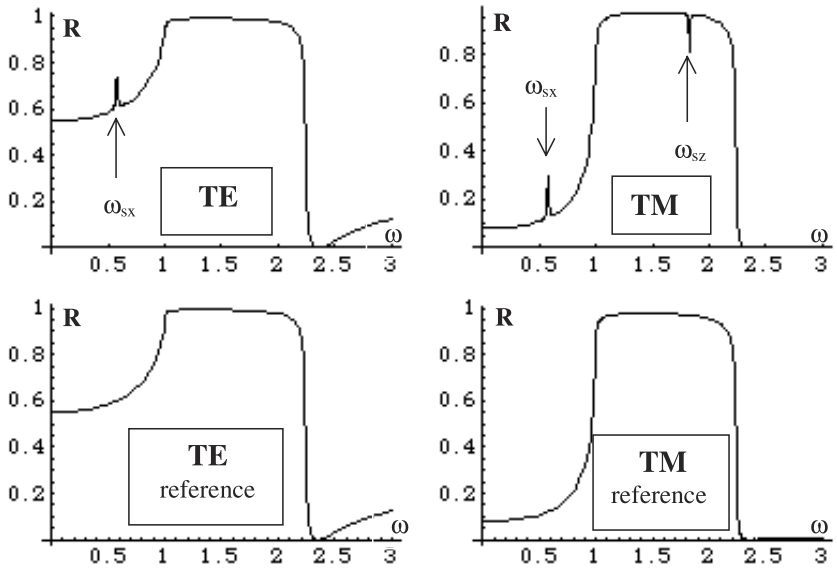

Figure 4. An overview of the TE and TM computed reflection spectra for a semi-infinite medium $\theta = 60°$. The parameters used differ appreciably from the ones listed in table 1, in order to improve visibility: $\omega_t = 1$, $\omega_l = 2$, $\varepsilon_\infty = 3$, $S\Omega_0^2 = 1.88 \times 10^{29}$ nm^2 s^{-2} (instead of 10^{25} in table 1), $\gamma = 0.01$, $\Delta_X = \Delta_Z = -2.25$ nm. Lower line: reference (ε_b) spectra.

In addition, a detailed study shows that this peak of reflectivity is very sharp. The presence of damping does not shift the frequency but drastically affects the amplitude: for $\gamma = 0.01$, the R variation in the vicinity of ω_{sx} does not exceed 1%.

3.1.2. TM propagation. Here again the reflection spectrum does not significantly differ from the one obtained in the case of a conventional dielectric medium, except in narrow frequency intervals; the occurrence of these intervals depends upon the signs of δ_x and of δ_z. More specifically: for δ_x negative one finds a peak of reflectivity very close to the frequency

$$\omega_{sx} = \left(\omega_t^2 - \frac{s}{\delta_x^2}\right)^{1/2}$$

and for δ_z negative one finds a sharp reflectivity minimum very close to the frequency ω_{sz} where

$$\omega_{sz} = \left(\omega_l^2 - \frac{s}{\delta_z^2}\right)^{1/2}. \tag{23}$$

This last frequency also corresponds to a solution for a surface mode at zero wavevector in the electrostatic approximation [17]. More precisely, a careful examination of the reflectivity spectrum around ω_{sz} in the absence of damping shows that this spectrum suffers a narrow oscillation with a $R = 1$ maximum immediately followed by a deep minimum. However, we have to note that this feature near ω_{sz} is extremely small when using the values of the parameters listed in table 1.

In figure 4, to clearly illustrate the above results, we show spectra covering a large frequency range obtained with modified values of ω_l and of s, which enhance the singularities in the vicinity of ω_{sx} and that of ω_{sz}.

To an excellent approximation the effects of the surface terms δ_x and δ_z are independent of each other and occur in different frequency ranges. As can be observed in figure 5, both δ coefficients provide contributions when and only when they are negative.

In the TM case, the expression for the reflectivity is less simple than in the TE configuration (see the appendix). However, its variation near ω_{sx} and ω_{sz} can be explained.

To conclude, the variation of the TM reflectivity spectrum of a semi-infinite medium versus the frequency in the paraelectric phase provides signatures of the occurrence of negative extrapolation lengths. Unfortunately, with a damping γ exceeding about 1%, which practically always occurs, the expected effects are presumably too weak to allow experimental observation. We have performed some complementary calculations which indicate that the attenuated reflection configuration does not significantly improve the observability of the surface terms.

3.2. Thin films

As pointed out above, the derivation of the surface parameters from the optical study of semi-infinite pieces of ferroelectrics is presumably subject to experimental difficulties, due to the weakness of the expected effects. In contrast, we show in this subsection that spatial dispersion combined with surface terms can give rise to large effects in thin films. Due to optical interferences the analysis of the reflection spectra is more complicated in thin films. Fortunately, when $\Omega D/c$ $(=\omega d) \ll 1$, most of the typical oscillations related to the phase variations classically observed in conventional plates disappear and one is left with the residual contributions arising from spatial dispersion combined with surface energy terms. With the parameter used ($D_0 = 30$ μm) the $\omega d \ll 1$ condition is realized for D smaller than a few hundreds of nanometres, which corresponds to films with interesting potential applications. However, this condition has to be carefully tested since the pertinent optical paths cannot be simply written as $\mathrm{Re}(q_i d)/2\pi$ but appear as $\mathrm{Re}(q_m d)/2\pi$ (with $m = 1, 2, 3$) and can then rise to large values, even when $\omega d \ll 1$. General expressions for the reflection and the transmission coefficients (respectively r and t) are given in the appendix. In the following, we often choose to show and comment on the reflectivity spectra. The transmission coefficient T of the intensity

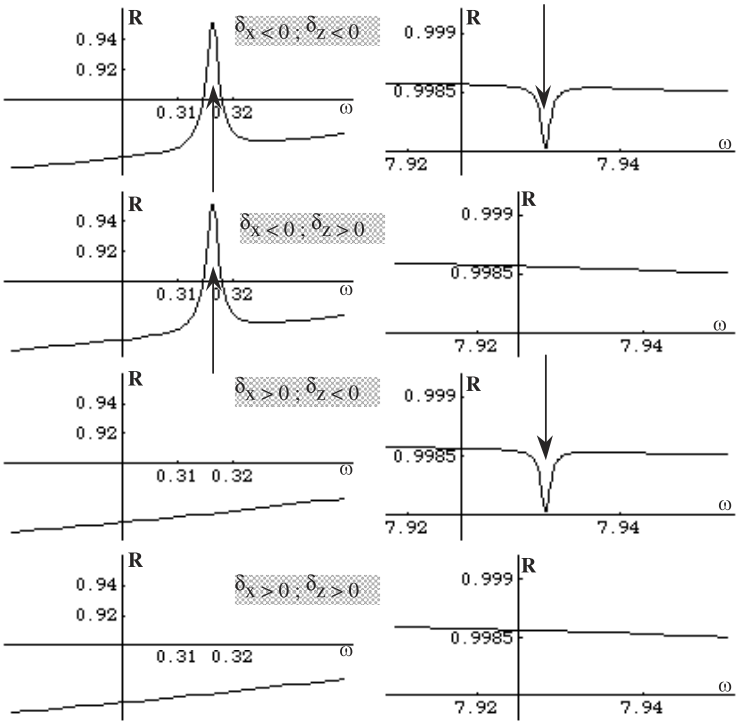

Figure 5. Sharp features of the TM computed reflection spectra in a semi-infinite medium: the dependence on the signs of the extrapolation lengths. $\theta = 60°$; $\gamma = 0.01$; $|\Delta_X| = |\Delta_Z| = 5$ nm.

is deduced from the transmission coefficient t of the amplitude of the electric field through the expressions $T = (\{\varepsilon_2/\varepsilon_1 - \sin^2\theta\}/\{1 - \sin^2\theta\})^{0.5} tt^*$. Note that T is equal to $(1 - R)$ in the absence of damping ($\gamma = 0$) but that it can appreciably differ from $(1 - R)$ even with the small γ values generally assumed in the present study.

3.2.1. TE propagation.

Free symmetric thin film. Figure 6 shows some computed reflection spectra of symmetrical thin films of thickness 30 and 90 nm, surrounded by vacuum ($\varepsilon_1 = \varepsilon_2 = 1$), in the case of negative δ_x ($\Delta_X = \Delta_{X,1} = \Delta_{X,2} = -5$ nm), without and with damping ($\gamma = 0$, 0.01, 0.1, 0.2, i.e. $\gamma_r = 0$, 0.022, 0.22, 0.45). They markedly differ from the ones obtained using the reference permittivity ε_b which are also shown for comparison. For larger values of γ the difference becomes very small and, presumably, undetectable. In the reference case the spectra are approximately centred around a maximum at ω_t ($R = 1$ in the absence of damping); in the films studied, for $\gamma = 0$ they present a well defined structure with several maxima at very different frequencies. Note that these frequencies are very close to the calculated ones for the even surface and guided modes in the electrostatic approximation at zero wavevector (equations (23) in [17]), namely

$$\omega_{ex,\{p\}} = (\omega_t^2 + s\chi_{ex,\{p\}}^2)^{1/2} \qquad p = 0, 1, 2, 3, \ldots \tag{24}$$

where $\chi_{ex,\{p\}}$ is the solution of

$$\chi\delta_x \sin[\chi d/2] - \cos[\chi d/2] = 0. \tag{25}$$

By convention, $p = 0$ corresponds to the purely imaginary solution for χ, when it exists, i.e. when $\delta_x < 0$: the frequency involved is smaller than ω_t and corresponds to a surface mode. When $|\delta_x|/d \ll 1$, the frequency of this mode is given approximately by equation (22). The other p values are related to real solutions and correspond to guided modes. A careful study of the spectra also allows one to detect extremely sharp oscillations around the frequencies of the odd modes, which are written as

$$\omega_{ox,\{p\}} = (\omega_t^2 + s\chi_{ox,\{p\}}^2)^{1/2} \qquad p = 0, 1, 2, 3, \ldots \tag{26}$$

where $\chi_{ox,\{p\}}$ is the solution of

$$\chi\delta_x \cos[\chi d/2] + \sin[\chi d/2] = 0. \tag{27}$$

Due to this sharpness they do not appear in figure 6. When damping is taken into account the features related to the odd modes are no longer detectable and, as regards the even modes, the small p values give rise to marked maxima (see ω_{sx} ($p = 0$) and $p = 1$ in figure 6) but the related contributions vanish when p increases. In the case of positive δ_x, the surface mode does not exist but the even guided modes are still observable: the reflection spectrum differs only weakly from the reference spectrum (see figure 7). In figure 8 we show the transmission spectra for two films of thickness 30 nm with $\delta_x = -5$ and +5 nm, respectively, assuming $\gamma = 0.01$ in both cases; as expected, the frequencies of the minima correspond to the frequencies of the above mentioned even surface and/or guided modes.

The above described singularities persist when D is varied but their frequencies (as expected) and their intensities change, as illustrated in figure 6. In contrast, the sweeping of k through the variation of the angle of incidence or through the simulation of attenuated reflectivity measurements does not modify the frequencies but does, indeed, allow one to change the general aspect of the spectra.

The expression for r in the absence of damping provides some explanation for the above described results. One finds

$$r = \tfrac{1}{2}\left\{ \frac{(q_i\cos[\varphi_1] + \mathrm{i}q_1\sin[\varphi_1])(q_1^2 - g^2)(\delta_x q_2 \sin[\varphi_2] - \cos[\varphi_2]) - (q_i\cos[\varphi_2] + \mathrm{i}q_2\sin[\varphi_2])(q_2^2 - g^2)(\delta_x q_1 \sin[\varphi_1] - \cos[\varphi_1])}{(q_i\cos[\varphi_1] - \mathrm{i}q_1\sin[\varphi_1])(q_1^2 - g^2)(\delta_x q_2 \sin[\varphi_2] - \cos[\varphi_2]) - (q_i\cos[\varphi_2] - \mathrm{i}q_2\sin[\varphi_2])(q_2^2 - g^2)(\delta_x q_1 \sin[\varphi_1] - \cos[\varphi_1])} \right.$$
$$\left. + \frac{(q_i\sin[\varphi_1] - \mathrm{i}q_1\cos[\varphi_1])(q_1^2 - g^2)(\delta_x q_2 \cos[\varphi_2] + \sin[\varphi_2]) - (q_i\sin[\varphi_2] - \mathrm{i}q_2\cos[\varphi_2])(q_2^2 - g^2)(\delta_x q_1 \cos[\varphi_1] + \sin[\varphi_1])}{(q_i\sin[\varphi_1] + \mathrm{i}q_1\cos[\varphi_1])(q_1^2 - g^2)(\delta_x q_2 \cos[\varphi_2] + \sin[\varphi_2]) - (q_i\sin[\varphi_2] + \mathrm{i}q_2\cos[\varphi_2])(q_2^2 - g^2)(\delta_x q_1 \cos[\varphi_1] + \sin[\varphi_1])} \right\} \tag{28}$$

where

$$\varphi_1 = \frac{q_1 d}{2}; \qquad \varphi_2 = \frac{q_2 d}{2}. \tag{29}$$

The transmission coefficient t is simply obtained by reversing the sign of the second term inside the external parentheses { }.

Let us evaluate r when, for instance, in equation (29) one states

$$\delta_x q_1 \sin[q_1 d/2] - \cos[q_1 d/2] = 0. \tag{30}$$

Expression (30) is identical to equation (25) which allows one to calculate the frequencies of the surface and of the guided modes at zero wavevector in the electrostatic approximation using equation (24). As pointed out in the preceding section the exact frequencies of these modes are very close to the values derived in the electrostatic approximation and show a very small dispersion versus k. Consequently, when it exists, the imaginary solution of equation (30) provides a q_1 value corresponding to a frequency which practically identifies itself with that of the even surface mode evaluated at zero wavevector under this approximation. It immediately results from equation (30) that the first term inside the brackets in equation (28)

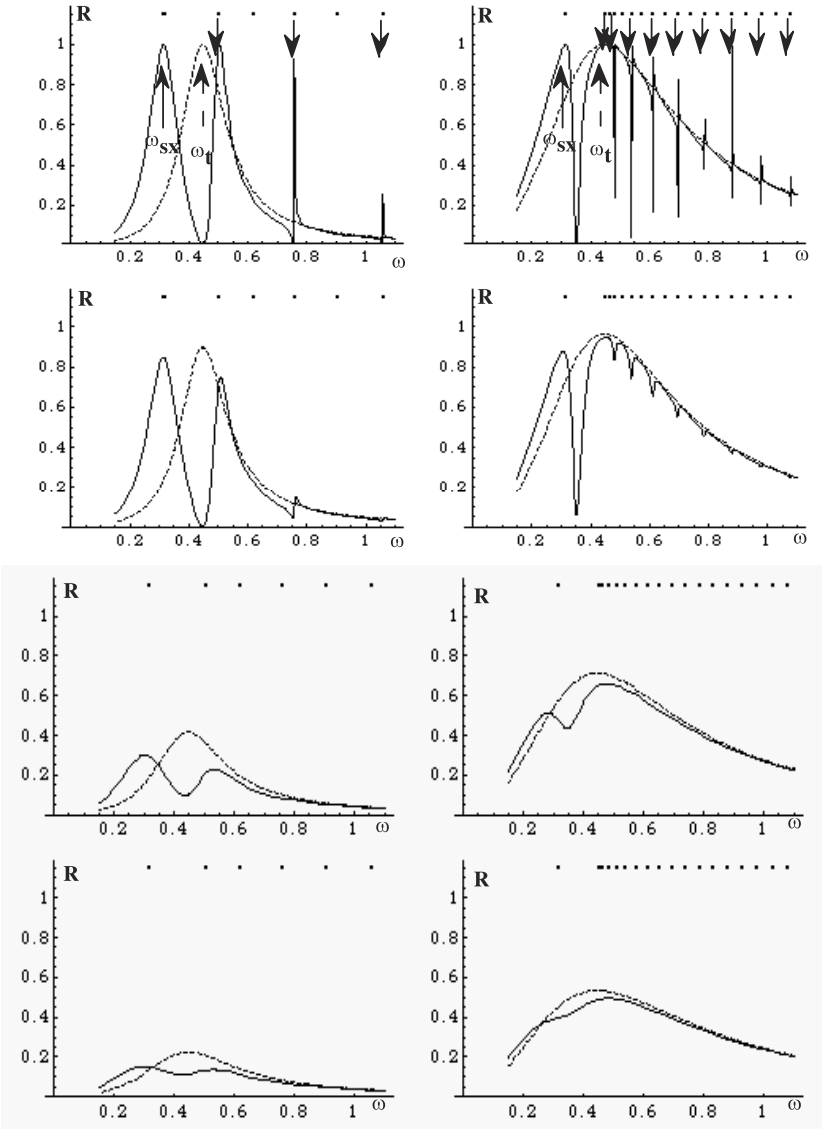

Figure 6. TE computed reflection spectra of thin films with a negative extrapolation length, surrounded by vacuum: $\theta = 30°$; $\Delta_X = -5$ nm. Thicknesses: 30 nm (left column) and 90 nm (right column). Damping: $\gamma = 0, 0.01, 0.1, 0.2$ (from top to bottom). The broken curves show the reference (ε_b) spectra. The full dots indicate the positions of the surface and of the guided modes, calculated at zero wavevector in the electrostatic approximation. The arrows indicate the positions of the even surface mode and of the even guided modes.

is of modulus 1—due to the fact that, in the frequency range explored, $|g^2 - q_1^2| \ll |g^2 - q_2^2|$, the second term inside the brackets is approximately equal to the first one and, consequently, r is of modulus 1, which means that $R = 1$. An analogous argument starting from the replacement of q_1 by q_2 in equation (30) can be developed for the even guided modes.

With the values of the parameters used in figure 6, $-\delta_x$ is significantly smaller than d: it results that the first frequency maximum only weakly depends on d and is approximately given

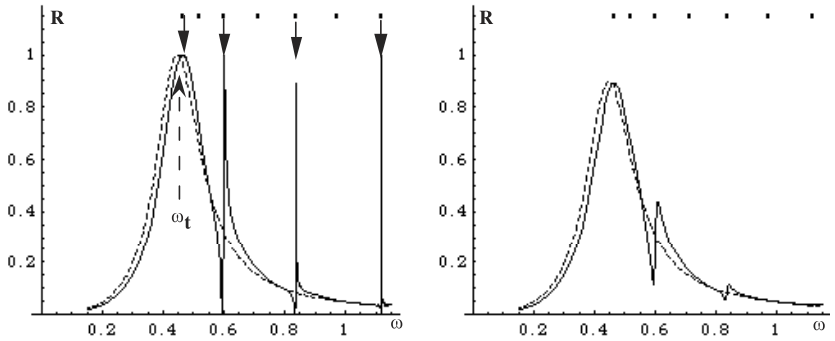

Figure 7. TE computed reflection spectra of a thin film with a positive extrapolation length, surrounded by vacuum: $\theta = 30°$; $\Delta_X = +5$ nm. Thickness: 30 nm. Damping: $\gamma = 0$ (left) and $\gamma = 0.01$ (right). The broken curves show the reference (ε_b) spectra. The full dots indicate the positions of the surface and of the guided modes, calculated at zero wavevector in the electrostatic approximation. The arrows indicate the positions of the even surface mode and of the even guided modes.

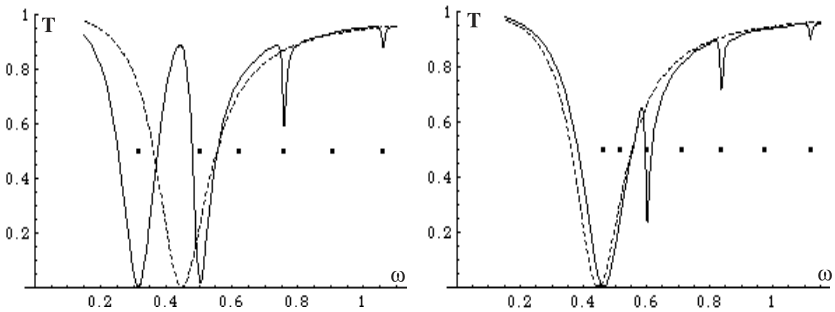

Figure 8. TE computed transmission spectra of thin films with negative or positive extrapolation lengths, surrounded by vacuum. Thickness: 30 nm; $\theta = 30°$. Damping: $\gamma = 0.01$; $\Delta_X = -5$ nm (left) and $\Delta_X = +5$ nm (right). The broken curves show the reference (ε_b) spectra. The full dots indicate the positions of the surface and of the guided modes, calculated at zero wavevector in the electrostatic approximation.

by (22): for negative δ_x subjected to $|\delta_x| \ll d$, the first maximum, which occurs below ω_t and is expected to be easily observed, allows one to evaluate s/δ_x^2. With the help of the other maxima related to the guided modes it is, in principle, possible to evaluate s and δ_x^2 separately, but the precision could be poor. Note that for large p values the frequencies of the guided modes only weakly depend upon δ_x and are given by

$$\omega_{ex,\{p\}} = \left(\omega_t^2 + \frac{4\pi^2 s}{d^2} p^2\right)^{1/2}. \tag{31}$$

When the studied extrapolation length is positive, the determination of δ_x and of s is not expected to be easy: however, due to the features arising from the guided modes, this determination is not hopeless.

Thin film on a substrate. We now consider the case of a film lying on a semi-infinite substrate: this system generally possesses two distinct tangential extrapolation lengths $\delta_{x,1}$ and $\delta_{x,2}$. In the following we have chosen $\varepsilon_1 = 1$ (vacuum), as previously, and $\varepsilon_2 = \varepsilon_\infty$, but this choice

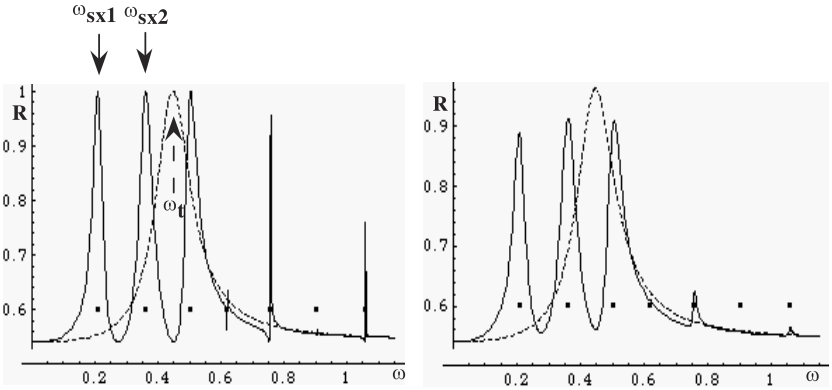

Figure 9. TE computed reflection spectra of a thin film lying on a substrate and showing two different negative extrapolation lengths: $\theta = 72°$; $\Delta_{X1} = -4$ nm, $\Delta_{X2} = -6$ nm, $\varepsilon_1 = 1$, $\varepsilon_2 = 5$. Thickness: 30 nm. Damping: $\gamma = 0$ (left) and $\gamma = 0.01$ (right). The full dots indicate the positions of the surface and of the guided modes, calculated at zero wavevector in the electrostatic approximation. The full arrows indicate the positions of the surface modes. The broken curves show the reference (ε_b) spectra.

is not essential. A computed reflection spectrum is shown in figure 9 for a film thickness of 30 nm without damping, in which both $\delta_{x,1}$ and $\delta_{x,2}$ are taken negative ($\Delta_{X,1} = -4$ nm, $\Delta_{X,2} = -6$ nm); here again, this spectrum significantly differs from the one obtained with a conventional dielectric medium presenting the reference permittivity ε_b and shows a set of several maxima. Figure 9 also provides the spectrum in the presence of a small damping ($\gamma = 0.01$); the above mentioned features are still present, but, as usual, the maxima decrease and the corresponding peaks broaden.

The frequencies of the maxima do not appreciably differ from the frequencies of the surface modes (when they exist) and of the guided modes at zero wavevector as evaluated in the electrostatic approximation. The calculation of these frequencies is a simple extension of the previously published one in the case of a symmetric surrounding [17]. The required solution is a linear combination of two exponential functions varying as $\exp[\mathrm{i}\chi z]$ and $\exp[-\mathrm{i}\chi z]$ where, from equations (5), χ is a solution of

$$\exp[2\mathrm{i}\chi d] = \frac{(\mathrm{i}\chi\delta_{x,1} - 1)(\mathrm{i}\chi\delta_{x,2} - 1)}{(\mathrm{i}\chi\delta_{x,1} + 1)(\mathrm{i}\chi\delta_{x,2} + 1)}. \tag{32}$$

The frequency related to any solution $\chi_{x,\{n\}}$ of equation (32) is written as

$$\omega_{x,\{n\}} = (\omega_{\mathrm{t}}^2 + s\chi_{x,\{n\}}^2)^{1/2}. \tag{33}$$

The imaginary χ values describe surface modes while the real ones define guided modes. Note that when $\delta_{x,1} = \delta_{x,2}$ equation (33) splits into two independent equations which separately provide the even and odd modes considered in the previous subsection. In the case of an unsymmetrical surrounding the modes are neither even nor odd. The existence of surface modes necessitates negative values of at least one of the extrapolation lines. A complete discussion is tedious. However, let us note that when $\delta_{x,1}$ and $\delta_{x,2}$ are both negative and subjected to $(|\delta_{x,1}| + |\delta_{x,2}|) < d$, two surface modes are present. This occurs in the case illustrated in figure 9: the two first maxima are related to these surface modes; the further maxima correspond to the guided modes. When $|\delta_{x,1}|/d \ll 1$ and $|\delta_{x,2}|/d \ll 1$ the frequencies

of the two surface modes are written approximately as

$$\omega_{sx,1} = \left(\omega_t^2 - \frac{s}{\delta_{x,1}^2}\right)^{1/2}; \qquad \omega_{sx,2} = \left(\omega_t^2 - \frac{s}{\delta_{x,2}^2}\right)^{1/2}. \tag{34}$$

Figure 9 illustrates this situation. In this case the values of $\delta_{x,1}$ and $\delta_{x,2}$ do not differ much from each other, which means that the surrounding does not differ much from a symmetrical one: it results that the succession of guided modes provokes alternate large and small perturbations (in the spectrum of a conventional dielectric medium). For large enough q values the frequency of the qth guided mode weakly depends on the extrapolation lengths and is approximately given by

$$\omega_q = \left(\omega_t^2 + \frac{\pi^2 s}{d^2}(q+1)^2\right)^{1/2}. \tag{35}$$

To summarize, in the same way as for the case of free symmetric films, it looks possible to derive the two extrapolation lengths and the spatial dispersion term for a thin film lying on a dielectric substrate. However, such an evaluation will be significantly easier when the extrapolation lengths are negative.

3.2.2. TM propagation. It is important to note that at normal incidence it is not possible to distinguish a TM from a TE spectrum. As long as one increases the angle of incidence, the differences between TE and TM spectra increase. In order to provide evidence for the characteristic features induced by the TM geometry it is then necessary to use a rather large angle of incidence (or to take advantage of an attenuated reflection mounting). At this stage we recall that, even for conventional dielectric thin films, the TE and TM reflection spectra show large differences: in the TE geometry the reflectivity is non-negligible only within a spectral range around the transverse ω_t frequency; in the TM polarization the reflectivity shows an additional broad peak of intensity in the vicinity of the longitudinal frequency ω_l.

As shown in figure 10, for the first spectral range around ω_t the TM reflectivity spectra reproduce the singularities appearing in the TE spectra: they only depend on the tangential extrapolation lengths and on the spatial dispersion coefficient s. In addition, in the high frequency region around ω_l and slightly above, additional features related to the normal extrapolation lengths (δ_z for a free symmetric film, $\delta_{z,1}$ and $\delta_{z,2}$ in the case of a film lying on a dielectric substrate) are expected. The frequencies for which these perturbations of the reflectivity appear are again found to lie very close to the frequencies of the surface and of the guided modes connected to ω_l (rather than ω_t as in the previous evaluations) calculated at zero wavevector in the electrostatic approximation. For instance, in the case of negative extrapolation lengths of low enough amplitude, reflectivity maxima occur at

$$\omega_{sz,1} = \left(\omega_l^2 - \frac{s}{\delta_{z,1}^2}\right)^{1/2} \qquad \text{and} \qquad \omega_{sz,2} = \left(\omega_l^2 - \frac{s}{\delta_{z,2}^2}\right)^{1/2}. \tag{36}$$

In figure 11 we present the transmission spectrum of a film of thickness 30 nm with a $\gamma = 0.01$ damping factor; the frequency minima now lie at the maxima of the reflection spectrum (see figure 10), as expected. Here again, in the case of a free thin film, only frequencies of the even modes are expected to be detectable. Practically, the effects of the tangential extrapolation length are independent of those of the normal extrapolation length, as is the case for the semi-infinite medium studied in the previous section. However, note that the flattening related to the damping is much more efficient for the singularities associated with δ_z than for those associated with δ_x. The general expressions for r and t are easily derived (see the appendix) but they are rather heavy and commenting on them is tedious work.

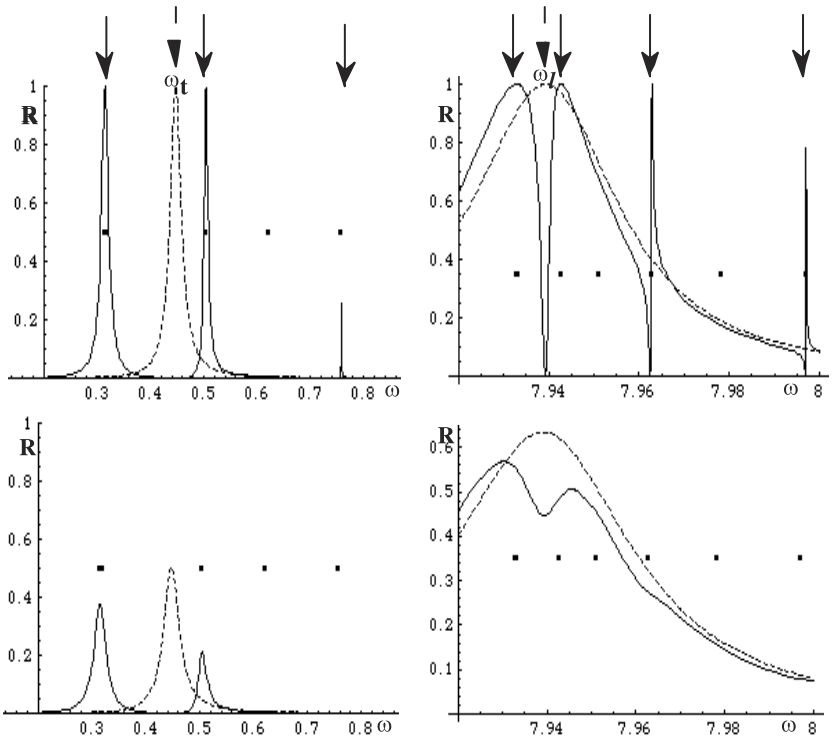

Figure 10. TM reflection spectra of a thin film with negative extrapolation lengths Δ_X and Δ_Z, surrounded by vacuum; $\theta = 81°$; $\Delta_X = -5$ nm, $\Delta_Z = -5$ nm. Thickness: 30 nm. Damping: $\gamma = 0$ (upper row) and $\gamma = 0.01$ (lower row). Spectral ranges: around ω_t (left column) and around ω_l (right column). The broken curves show the reference (ε_b) spectra. The full dots indicate the positions of the surface and of the guided modes, calculated at zero wavevector in the electrostatic approximation. The arrows indicate the positions of the even surface mode and of the even guided modes.

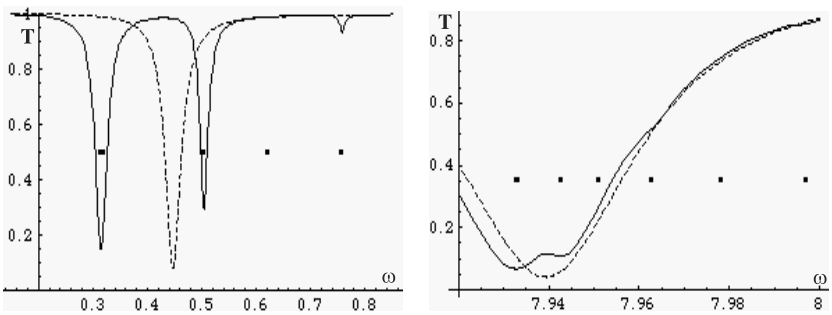

Figure 11. TM transmission spectra of a thin film with negative extrapolation lengths Δ_X and Δ_Z, surrounded by vacuum; $\theta = 81°$; $\Delta_X = -5$ nm, $\Delta_Z = -5$ nm. Thickness: 30 nm. Damping: $\gamma = 0.01$. Spectral ranges: around ω_t (left) and around ω_l (right). The broken curves show the reference (ε_b) spectra. The full dots indicate the positions of the surface and of the guided modes, calculated at zero wavevector in the electrostatic approximation.

In figure 12, results for a film of thickness 30 nm lying on a dielectric substrate are presented, assuming different negative values of the extrapolation lengths on each side ($\Delta_{X,1} = \Delta_{Z,1} = -4$ nm, $\Delta_{X,2} = \Delta_{Z,2} = -6$ nm), with $\gamma = 0.01$. As previously mentioned

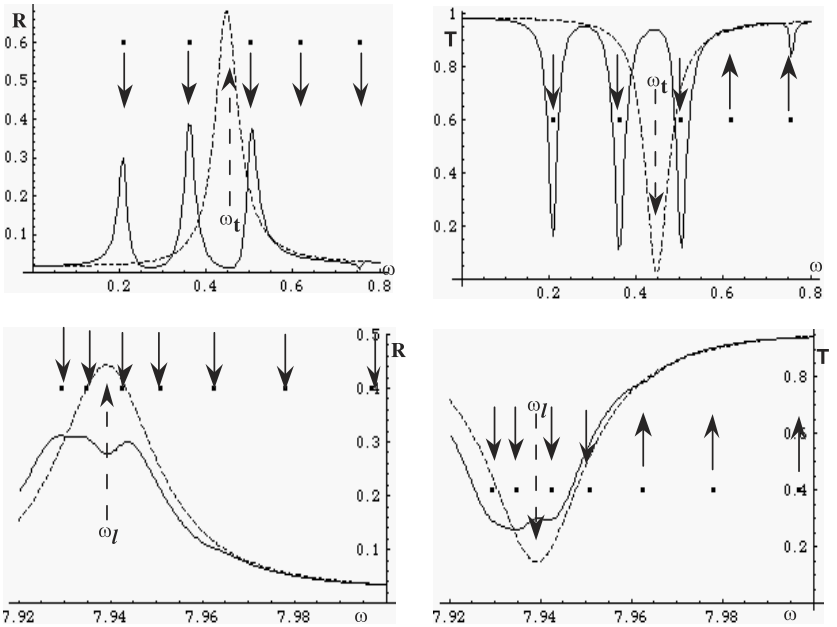

Figure 12. TM computed reflection (left column) and transmission (right column) spectra of a thin film lying on a substrate and showing different negative extrapolation lengths on each side; $\theta = 81°$; $\Delta_{X,1} = \Delta_{Z,1} = -4$ nm, $\Delta_{X,2} = \Delta_{Z,2} = -6$ nm, $\varepsilon_1 = 1$, $\varepsilon_2 = 5$. Thickness: 30 nm. Damping: $\gamma = 0.01$. Spectral ranges: around ω_t (upper row) and around ω_l (lower row). The broken curves show the reference (ε_b) spectra. The full dots indicate the positions of the surface and of the guided modes, calculated at zero wavevector in the electrostatic approximation. The arrows indicate the positions of the surface modes and of the guided modes.

Table 2. A review of the expected optical singularities. (In symmetrically surrounded films, the odd modes give rise to very weak and presumably undetectable singularities.)

	Expected singularity types in spectra	
Systems	TE	TM
Semi-infinite medium (reflection)	* Surface: ω_{sx} (for $\delta_x < 0$)	* Surface: ω_{sx} (for $\delta_x < 0$) ** Surface: ω_{sz} (for $\delta_z < 0$)
Symmetrically surrounded film (reflection and transmission)	* Surface: even $\omega_{ex,\{p=0\}}$ (for $\delta_x < 0$) ** Guided: even $\omega_{ex,\{p\neq 0\}}$	* Surface: even $\omega_{ex,\{p=0\}}$ (for $\delta_x < 0$) + even $\omega_{ez,\{p=0\}}$ (for $\delta_z < 0$) ** Guided: even $\omega_{ex,\{p\neq 0\}}$ + even guided $\omega_{ez,\{p\neq 0\}}$
Unsymmetrically surrounded film (reflection and transmission)	* Surface: (for $\delta_{x,1} < 0$ or $\delta_{x,2} < 0$), one or two frequencies (*see the text*) ** Guided: no restriction	* Surface: (for $\delta_{x,1} < 0$ or $\delta_{x,2} < 0$), one or two frequencies + surface: (for $\delta_{z,1} < 0$ or $\delta_{z,2} < 0$), one or two frequencies ** Guided: no restriction

for the TE case, the whole set of surface and guided modes is now implied. The features related to $\delta_{z,1}$ and $\delta_{z,2}$ remain more affected by the damping.

In principle, it would be possible to evaluate Δ_Z (or $\Delta_{Z,1}$ and $\Delta_{Z,2}$): however, the intensity variations are smaller in the spectral region concerned close to ω_l than around ω_t and we thus believe that the experimental determinations will be difficult, especially in the case of positive extrapolation lengths.

4. Conclusion

We have discussed the dependence of the optical properties of surface and thin films upon the parameters which allow one to monitor the size effects on nanostructured ferroelectric systems. We have given evidence that, when the damping constant γ does not exceed a few tenths, reflection and transmission spectra are expected to be significantly affected, even in the paraelectric state above the temperature of the transition. The main expected perturbations are schematically presented in table 2. We have shown that both the extrapolation lengths and the spatially dispersive gradient terms appearing in the free energy modify the reflectivity and the transmittivity of thin films. However, for film thicknesses not exceeding a few hundreds of nanometres, in the absence of surface energy (i.e. in the limit of vanishing inverse extrapolation lengths) the gradient terms only very weakly contribute to the modification of the spectra, at least for the generally accepted orders of magnitude of these terms. In contrast, the occurrence of extrapolation lengths with absolute values of a few nanometres has a strong effect on the spectra: they introduce reflection maxima (and, simultaneously, transmission minima) at frequencies which are very easy to evaluate since they practically coincide with the frequencies of the surface and guided modes of the structures studied calculated at zero wavevector in the electrostatic approximation. The infrared spectra are then expected to allow a direct measurement of the tangential and normal algebraic interfacial extrapolation lengths and of the dispersive gradient terms. It is apparent from our discussion that this technique would be particularly convenient for the detection of negative extrapolation lengths, the existence of which is still a subject of controversy. However, it must be noted that an overdamping of the soft mode is frequently observed; this happens for instance in $BaTiO_3$ [21]. Such an overdamping prevents the optical detection of the above discussed dispersion and surface effects. In contrast, reasonably small values of γ have been measured in other ferroelectrics, at least for the ordered phase; this is the case for $PbTiO_3$, for example [22–25]. One can then hope that, using appropriate materials, it will be possible to get access to surface and spatial dispersion terms. On the other hand, it is of interest to note that, in principle, the calculations developed in the present paper are able to describe the combined effect of the dispersion of the optical phonons and hypothetical interface energy terms on the optical properties of standard dielectric thin film: however, the values of the dispersion parameter S usually found are presumably too small to induce easily experimentally detectable features. Infrared spectroscopy was successfully used in the past in order to study the softening of the vibrational dynamics in the vicinity of the phase transitions of ferroelectric bulk materials. More recently, it was extended to the search for size effects in thin films [26]. We hope that the present work will encourage new experimental investigations in this domain.

Acknowledgment

We are pleased to thank V Dvorák from the Institute of Physics of the Academy of Sciences of the Czech Republic for fruitful discussions throughout this work.

Appendix. Expressions for the reflection and transmission coefficients

The continuity of the tangential component of the electric field $\mathbf{E}$ (E_Y for the TE solutions, E_X for the TM ones) and of the magnetic field $\mathbf{H}$ (H_X for the TE solutions, H_Y for the TM ones) and the boundary conditions related to the surface terms in the free energy (involving Δ_X only for the TE solutions, both Δ_X and Δ_Z for the TM ones) provide the appropriate numbers of linear equations required in order to derive r and t.

A.1. Semi-infinite medium

For the TE propagation r was given in equation (19). For the TM propagation one finds

$$\begin{aligned} r = {} & \{(q_1 q_\mathrm{i} - k^2)(q_\mathrm{i} - q_1)(q_1^2 - g^2)A_1 - (q_2 q_\mathrm{i} - k^2) \\ & \times (q_\mathrm{i} - q_2)(q_2^2 - g^2)A_2 - k(q_\mathrm{i}^2 + k^2)(q_3^2 - g^2)A_3\} \\ & \times \{(q_1 q_\mathrm{i} + k^2)(q_\mathrm{i} + q_1)(q_1^2 - g^2)A_1 - (q_2 q_\mathrm{i} + k^2)(q_\mathrm{i} + q_2)(q_2^2 - g^2)A_2 \\ & - k(q_\mathrm{i}^2 + k^2)(q_3^2 - g^2)A_3\}^{-1} \end{aligned} \tag{A.1}$$

with

$$\begin{aligned} A_1 &= q_2 q_3 (q_2 + \mathrm{i}/\delta_x)(q_3 + \mathrm{i}/\delta_z) + k^2 (q_2 + \mathrm{i}/\delta_z)(q_3 + \mathrm{i}/\delta_x) \\ A_2 &= q_1 q_3 (q_1 + \mathrm{i}/\delta_x)(q_3 + \mathrm{i}/\delta_z) + k^2 (q_1 + \mathrm{i}/\delta_z)(q_3 + \mathrm{i}/\delta_x) \\ A_3 &= q_1 k (q_1 + \mathrm{i}/\delta_x)(q_2 + \mathrm{i}/\delta_z) - q_2 k (q_1 + \mathrm{i}/\delta_z)(q_2 + \mathrm{i}/\delta_x). \end{aligned}$$

It can be easily seen that for $k = 0$, expression (A.1) reduces to equation (19) at $k = 0$, as expected.

A.2. Thin film

A.2.1. TE propagation. The r and t values for a TE propagation with a thin film lying on a substrate are given by

$$r = \frac{A_{22} D_1 - A_{12} D_2}{A_{11} A_{22} - A_{12} A_{21}}; \qquad t = \frac{A_{11} D_2 - A_{21} D_1}{A_{11} A_{22} - A_{12} A_{21}} \tag{A.2}$$

where

$$\begin{aligned} A_{11} = {} & U\{(q_2 \cos[\varphi_2] + \sigma \sin[\varphi_2]/2)(q_1^2 - g^2)(\mathrm{i}q_1 \cos[\varphi_1] + q_\mathrm{i} \sin[\varphi_1]) \\ & - (q_1 \cos[\varphi_1] + \sigma \sin[\varphi_1]/2)(q_2^2 - g^2)(\mathrm{i}q_2 \cos[\varphi_2] + q_\mathrm{i} \sin[\varphi_2])\} \\ & + V\Sigma/2\{\cos[\varphi_2](q_1^2 - g^2)(-\mathrm{i}q_1 \sin[\varphi_1] + q_\mathrm{i} \cos[\varphi_1]) \\ & - \cos[\varphi_1](q_2^2 - g^2)(-\mathrm{i}q_2 \sin[\varphi_2] + q_\mathrm{i} \cos[\varphi_2])\} \\ A_{12} = {} & -U\{(q_2 \cos[\varphi_2] + \sigma \sin[\varphi_2]/2)(q_1^2 - g^2)(\mathrm{i}q_1 \cos[\varphi_1] + q_t \sin[\varphi_1]) \\ & - (q_1 \cos[\varphi_1] + \sigma \sin[\varphi_1]/2)(q_2^2 - g^2)(\mathrm{i}q_2 \cos[\varphi_2] + q_t \sin[\varphi_2])\} \\ & + V\Sigma/2\{\cos[\varphi_2](q_1^2 - g^2)(-\mathrm{i}q_1 \sin[\varphi_1] + q_t \cos[\varphi_1]) \\ & - \cos[\varphi_1](q_2^2 - g^2)(-\mathrm{i}q_2 \sin[\varphi_2] + q_t \cos[\varphi_2])\} \\ A_{21} = {} & V\{(q_2 \sin[\varphi_2] - \sigma \cos[\varphi_2]/2)(q_1^2 - g^2)(-\mathrm{i}q_1 \sin[\varphi_1] + q_\mathrm{i} \cos[\varphi_1]) \\ & - (q_1 \sin[\varphi_1] - \sigma \cos[\varphi_1]/2)(q_2^2 - g^2)(-\mathrm{i}q_2 \sin[\varphi_2] + q_\mathrm{i} \cos[\varphi_2])\} \\ & - U\Sigma/2\{\sin[\varphi_2](q_1^2 - g^2)(\mathrm{i}q_1 \cos[\varphi_1] + q_\mathrm{i} \sin[\varphi_1]) \\ & - \sin[\varphi_1](q_2^2 - g^2)(\mathrm{i}q_2 \cos[\varphi_2] + q_\mathrm{i} \sin[\varphi_2])\} \\ A_{22} = {} & V\{(q_2 \sin[\varphi_2] - \sigma \cos[\varphi_2]/2)(q_1^2 - g^2)(-\mathrm{i}q_1 \sin[\varphi_1] + q_t \cos[\varphi_1]) \\ & - (q_1 \sin[\varphi_1] - \sigma \cos[\varphi_1]/2)(q_2^2 - g^2)(-\mathrm{i}q_2 \sin[\varphi_2] + q_t \cos[\varphi_2])\} \\ & + U\Sigma/2\{\sin[\varphi_2](q_1^2 - g^2)(\mathrm{i}q_1 \cos[\varphi_1] + q_t \sin[\varphi_1]) \\ & - \sin[\varphi_1](q_2^2 - g^2)(\mathrm{i}q_2 \cos[\varphi_2] + q_t \sin[\varphi_2])\} \\ D_1 = {} & U\{(q_2 \cos[\varphi_2] + \sigma \sin[\varphi_2]/2)(q_1^2 - g^2)(-\mathrm{i}q_1 \cos[\varphi_1] + q_\mathrm{i} \sin[\varphi_1]) \\ & - (q_1 \cos[\varphi_1] + \sigma \sin[\varphi_1]/2)(q_2^2 - g^2)(-\mathrm{i}q_2 \cos[\varphi_2] + q_\mathrm{i} \sin[\varphi_2])\} \\ & + V\Sigma/2\{\cos[\varphi_2](q_1^2 - g^2)(\mathrm{i}q_1 \sin[\varphi_1] + q_\mathrm{i} \cos[\varphi_1]) \end{aligned} \tag{A.3}$$

$$
\begin{aligned}
&- \cos[\varphi_1](q_2^2 - g^2)(\mathrm{i}q_2 \sin[\varphi_2] + q_\mathrm{i} \cos[\varphi_2])\} \\
D_2 = V\{&(q_2 \sin[\varphi_2] - \sigma \cos[\varphi_2]/2)(q_1^2 - g^2)(\mathrm{i}q_1 \sin[\varphi_1] + q_\mathrm{i} \cos[\varphi_1]) \\
&- (q_1 \sin[\varphi_1] - \sigma \cos[\varphi_1]/2)(q_2^2 - g^2)(\mathrm{i}q_2 \sin[\varphi_2] + q_\mathrm{i} \cos[\varphi_2])\} \\
&- U\Sigma/2\{\sin[\varphi_2](q_1^2 - g^2)(-\mathrm{i}q_1 \cos[\varphi_1] + q_\mathrm{i} \sin[\varphi_1]) \\
&- \sin[\varphi_1](q_2^2 - g^2)(-\mathrm{i}q_2 \cos[\varphi_2] + q_\mathrm{i} \sin[\varphi_2])\}
\end{aligned}
$$

with

$$
\begin{aligned}
U &= q_1 \cos[\varphi_2] \sin[\varphi_1] - q_2 \cos[\varphi_1] \sin[\varphi_2] \\
V &= q_1 \cos[\varphi_1] \sin[\varphi_2] - q_2 \cos[\varphi_2] \sin[\varphi_1]
\end{aligned}
\tag{A.4}
$$

and

$$
\sigma = \frac{\delta_{x,1} + \delta_{x,2}}{\delta_{x,1}\,\delta_{x,2}}; \qquad \Sigma = \frac{\delta_{x,1} - \delta_{x,2}}{\delta_{x,1}\,\delta_{x,2}}. \tag{A.5}
$$

In the above equations $q_t = (\varepsilon_2\omega^2 - k^2)^{1/2}$ stands for the normal component of the transmitted wavevector. In the case of symmetrical surroundings ($\varepsilon_1 = \varepsilon_2$), the expression for r in equations (A.2) reduces to equation (28).

A.2.2. TM propagation. The general expressions for an unsymmetrical surrounding are rather complicated. In the case of a symmetrical surrounding, one obtains simpler equations (A.6):

$$
\begin{aligned}
r = \frac{1}{2}\Bigg\{&\frac{\alpha_{1a}(q_1^2 - g^2)M_1 - \alpha_{2a}(q_2^2 - g^2)M_2 - \alpha_3(q_3^2 - g^2)M_3}{\alpha_{1b}(q_1^2 - g^2)M_1 - \alpha_{2b}(q_2^2 - g^2)M_2 - \alpha_3(q_3^2 - g^2)M_3} \\
&+ \frac{\beta_{1b}(q_1^2 - g^2)N_1 - \beta_{2b}(q_2^2 - g^2)N_2 - \beta_3(q_3^2 - g^2)N_3}{\beta_{1a}(q_1^2 - g^2)N_1 - \beta_{2a}(q_2^2 - g^2)N_2 - \beta_3(q_3^2 - g^2)N_3}\Bigg\} \\
t = \frac{1}{2}\Bigg\{&\frac{\alpha_{1a}(q_1^2 - g^2)M_1 - \alpha_{2a}(q_2^2 - g^2)M_2 - \alpha_3(q_3^2 - g^2)M_3}{\alpha_{1b}(q_1^2 - g^2)M_1 - \alpha_{2b}(q_2^2 - g^2)M_2 - \alpha_3(q_3^2 - g^2)M_3} \\
&- \frac{\beta_{1b}(q_1^2 - g^2)N_1 - \beta_{2b}(q_2^2 - g^2)N_2 - \beta_3(q_3^2 - g^2)N_3}{\beta_{1a}(q_1^2 - g^2)N_1 - \beta_{2a}(q_2^2 - g^2)N_2 - \beta_3(q_3^2 - g^2)N_3}\Bigg\}
\end{aligned}
\tag{A.6}
$$

where

$$
\begin{aligned}
&\alpha_{ja} = q_j(k^2 + q_\mathrm{i}^2)\cos[\varphi_j] + \mathrm{i}q_\mathrm{i}(k^2 + q_j^2)\sin[\varphi_j] && (j = 1, 2) \\
&\alpha_{jb} = q_j(k^2 + q_\mathrm{i}^2)\cos[\varphi_j] - \mathrm{i}q_\mathrm{i}(k^2 + q_j^2)\sin[\varphi_j] && (j = 1, 2) \\
&\alpha_3 = k(k^2 + q_\mathrm{i}^2)\cos[\varphi_3] \qquad \text{with: } \varphi_3 = q_3 d/2 && \\
&\beta_{ja} = q_j(k^2 + q_\mathrm{i}^2)\sin[\varphi_j] + \mathrm{i}q_\mathrm{i}(k^2 + q_j^2)\cos[\varphi_j] && (j = 1, 2) \\
&\beta_{jb} = q_j(k^2 + q_\mathrm{i}^2)\sin[\varphi_j] - \mathrm{i}q_\mathrm{i}(k^2 + q_j^2)\cos[\varphi_j] && (j = 1, 2) \\
&\beta_3 = k(k^2 + q_\mathrm{i}^2)\sin[\varphi_3] &&
\end{aligned}
\tag{A.7}
$$

and

$$
\begin{aligned}
M_1 &= q_2q_3(q_2\sin[\varphi_2]-\cos[\varphi_2]/\delta_x)(q_3\cos[\varphi_3]+\sin[\varphi_3]/\delta_z)\\
&\quad + k^2(q_3\sin[\varphi_3]-\cos[\varphi_3]/\delta_x)(q_2\cos[\varphi_2]+\sin[\varphi_2]/\delta_z)\\
N_1 &= q_2q_3(q_2\cos[\varphi_2]+\sin[\varphi_2]/\delta_x)(q_3\sin[\varphi_3]-\cos[\varphi_3]/\delta_z)\\
&\quad + k^2(q_3\cos[\varphi_3]+\sin[\varphi_3]/\delta_x)(q_2\sin[\varphi_2]-\cos[\varphi_2]/\delta_z)\\
M_2 &= q_3q_1(q_1\sin[\varphi_1]-\cos[\varphi_1]/\delta_x)(q_3\cos[\varphi_3]+\sin[\varphi_3]/\delta_z)\\
&\quad + k^2(q_3\sin[\varphi_3]-\cos[\varphi_3]/\delta_x)(q_1\cos[\varphi_1]+\sin[\varphi_1]/\delta_z)\\
N_2 &= q_3q_1(q_1\cos[\varphi_1]+\sin[\varphi_1]/\delta_x)(q_3\sin[\varphi_3]-\cos[\varphi_3]/\delta_z)\\
&\quad + k^2(q_3\cos[\varphi_3]+\sin[\varphi_3]/\delta_x)(q_1\sin[\varphi_1]-\cos[\varphi_1]/\delta_z)\\
M_3 &= kq_1(q_1\sin[\varphi_1]-\cos[\varphi_1]/\delta_x)(q_2\cos[\varphi_2]+\sin[\varphi_2]/\delta_z)\\
&\quad - kq_2(q_2\sin[\varphi_2]-\cos[\varphi_2]/\delta_x)(q_1\cos[\varphi_1]+\sin[\varphi_1]/\delta_z)\\
N_3 &= kq_1(q_1\cos[\varphi_1]+\sin[\varphi_1]/\delta_x)(q_2\sin[\varphi_2]-\cos[\varphi_2]/\delta_z)\\
&\quad - kq_2(q_2\cos[\varphi_2]+\sin[\varphi_2]/\delta_x)(q_1\sin[\varphi_1]-\cos[\varphi_1]/\delta_z).
\end{aligned}
\tag{A.8}
$$

Here again, it is easily seen that when $k = 0$, expression (A.6) reduces to equation (28) at $k = 0$, as expected.

References

[1] Kretschmer R and Binder K 1979 *Phys. Rev.* B **20** 1065
[2] Tilley D R 1996 *Ferroelectric Thin Films: Synthesis and Basic Properties* ed C A Paz de Araujo, J F Scott and G W Taylor (London: Gordon and Breach)
[3] Tilley D R and Zeks B 1984 *Solid State Commun.* **49** 823
[4] Cottam M G, Tilley D R and Zeks B 1984 *J. Phys. C: Solid State Phys.* **17** 1793
[5] Ishikawa K, Yoshikawa K and Okada N 1988 *Phys. Rev.* B **37** 5852
[6] Scott J F 1988 *Physica* B **150** 160
[7] Wang Y G, Zhong W L and Zhang P L 1994 *Solid State Commun.* **90** 329
[8] Wang Y G, Zhong W L and Zhang P L 1994 *Solid State Commun.* **92** 519
[9] Wang C L and Smith S R P 1995 *J. Phys.: Condens. Matter* **7** 7163
[10] Li S, Eastman J A, Vetrone J M, Foster C M, Newnham R E and Cross L E 1997 *Japan. J. Appl. Phys.* **36** 5169
[11] Tybell T, Ahn C H and Triscone J M 1999 *Appl. Phys. Lett.* **75** 856
[12] Ghosez P and Rabe K M 2000 *Appl. Phys. Lett.* **76** 2767
[13] Junquera J and Ghosez P 2003 *Nature* **422** 506
[14] Chew K H, Ong L H, Osman J and Tilley D R 2001 *J. Opt. Soc. Am.* B **18** 1512
[15] Chew K H, Osman J, Stamps R L, Tilley D R and Webb J F 1999 *Integr. Ferroelectr.* **23** 161
[16] Maradudin A A and Mills D L 1973 *Phys. Rev.* B **7** 2787
[17] Jardin J-P, Moch P and Dvorák V 2002 *J. Phys.: Condens. Matter* **14** 1745
[18] Jardin J-P and Moch P 2003 *Ferroelectrics* **288** 71
[19] Fuchs R, Kliewer K L and Pardee W J 1966 *Phys. Rev.* **150** 589
[20] Ruppin R and Englman R 1970 *Rep. Prog. Phys.* **33** 149
[21] Vogt H, Sanjurjo J A and Rossbroich G 1982 *Phys. Rev.* B **26** 5904
[22] Burns G and Scott B A 1970 *Phys. Rev. Lett.* **25** 167
[23] Burns G and Scott B A 1972 *Phys. Rev.* B **7** 3088
[24] Fedorov I, Petzelt J, Zelezny V, Komandin G A, Volkov A A, Brooks K, Huang Y and Setter M 1995 *J. Phys.: Condens. Matter* **7** 4313
[25] Fu D S, Iwazaki H, Suzuki H and Ishikawa K 2000 *J. Phys.: Condens. Matter* **12** 399
[26] Petzelt J, Kuzel P, Rychetsky I, Pashkin A and Ostapchuk T 2003 *Ferroelectrics* **288** 169